

pubs.acs.org/Macromolecules Article

p-Type Semiconducting Ladder Poly(pyrrolobenzothiazine)s: Effects of N-Alkyl Side Chains on the Chain Conformation, Electronic Structure, and Charge Transport Properties

Sarah M. West, Duyen K. Tran, Jiajie Guo, Shinya E. Chen, David S. Ginger, and Samson A. Jenekhe*



Cite This: Macromolecules 2023, 56, 10222-10235



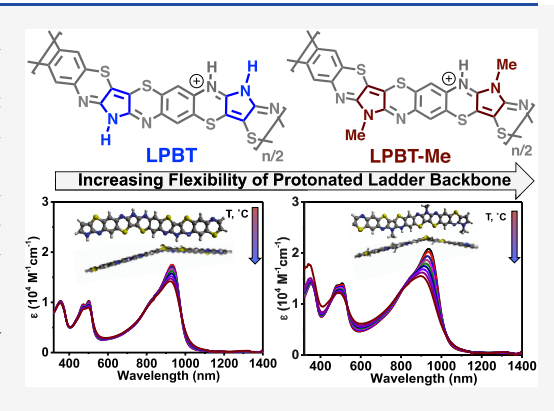
ACCESS I

III Metrics & More

Article Recommendations

Supporting Information

ABSTRACT: In this work, we show how *N*-alkyl substitution affects the chain conformation, electronic structure, and optical and charge transport properties of π -conjugated ladder poly(pyrrolobenzothiazines)s (LPBTs). We found that the π -conjugated backbones of the LPBTs have a donor—acceptor motif, which enabled a small bandgap of 1.5 eV that is unchanged by *N*-alkyl substitution. We found that partial protonation of the LPBTs in acid solutions resulted in increased backbone flexibility evidenced by thermochromism in solution and planar/nonplanar chain conformational variation with degree of protonation that we saw in density functional theory (DFT) calculations. The average field-effect hole mobility increased from 1.3×10^{-3} cm²/(V s) in LPBT-Me to 3.1×10^{-3} cm²/(V s) in LPBT, which can be explained by the increased crystallinity and decreased lattice disorder in LPBT. The results of our investigations of the solution and solid-state properties of the two ladder poly-



(pyrrolobenzothiazine)s provide new insights into the structure-property relationships of π -conjugated ladder polymers.

■ INTRODUCTION

It is well known that the backbone conformation of π conjugated polymers directly impacts their electronic structure and properties including molecular orbital distribution, reorganizational energy during charge transfer process, intermolecular transfer integrals, 1,2 and the degree of electronic delocalization. In contrast to semiflexible polymers that show conformational torsions and rotations along the single bonds that link the polymer repeat units, π -conjugated ladder polymers feature a double-stranded architecture that is thought to limit conformational distortions and promote backbone rigidity. $^{1,3-5}$ The most notable member of the π -conjugated ladder polymers, poly(benzimidazobenzophenanthroline) (BBL) (Chart 1), first synthesized in 1966 for aerospace applications due to its extremely high thermal and chemical stability, has been successfully used in a variety of organic electronic and optoelectronic applications over the past 3 decades.3,7-21 BBL and its derivatives are the only known examples of π -conjugated ladder polymers that have rigid-rod backbones in solution and solid state; 22-25 the scarcity is primarily because of the difficulty in the synthesis of π conjugated ladder polymers in general. 4,5,25-31 For example, in polymers such as BBL and ladder-type polyaniline derivatives,³² installing basic sites such as imine nitrogens in the backbone is a key design feature that enables either processing in protic acids or offers unique properties such as acid-doped conductivity. Beyond BBL, there is one other conjugated ladder polymer, called ladder poly(p-phenylene) (LPPP), that

Chart 1. Molecular Structures of π -Conjugated Ladder Polymers BBL, LPBT, and LPBT-Me, and Ladder Molecule PBRTZ

has been subjected to rigorous studies of its backbone conformation and persistence length.³⁴ Interestingly, it was found that LPPP has a wormlike conformation despite its ladder architecture, which means that LPPP showed bending

Received: August 4, 2023 Revised: November 21, 2023 Accepted: November 24, 2023 Published: December 13, 2023





fluctuations in solution.³⁴ There is a need to further explore the structure–property relationships of π -conjugated ladder polymers since it is evident that they do not exclusively have rigid-rod conformations as widely assumed.

An intriguing ladder small-molecule p-type semiconductor, PBBTZ³⁵ (Chart 1), which features an electron-rich, coplanar pyrrolobenzothiazine building block, was reported to exhibit high hole mobility (μ_h) values of 0.34 cm²/(V s) in polycrystalline thin-film organic field-effect transistors (OFET)³⁵ and 3.6 cm²/(V s) in single-crystal field-effect transistors.³⁶ These results suggested that incorporation of pyrrolobenzothiazine moieties into π -conjugated polymers could enable good charge transport properties. In 2012, a pyrrolobenzothiazine-based π -conjugated ladder polymer featuring 2-octyldodecyl solubilizing groups (PPBBTZ) was reported, although no charge transport properties or molecular geometry studies were reported.³⁷ Recently, the parent ladder poly(6*H*-pyrrolo[3,2-*b*:4,5-*b*']benzothiazine) (LPBT), without solubilizing alkyl chains, was reported; we note that this polymer was named 6H-pyrrolo[3,2-b:4,5-b']bis[1,4]benzothiazine ladder (PBBTL), which we believe is incorrectly derived from the model compound PBBTZ.²⁹ It was shown that LPBT has a highest occupied molecular orbital (HOMO) level of -5.0 eV and could be p-type doped with FeCl₃ to a moderate electrical conductivity of 1.54 S/cm and showed moderate thermoelectric properties.³⁰ Moreover, blends of ptype LPBT and n-type BBL have been used to fabricate pchannel and n-channel organic electrochemical transistors (OECTs), which gave μC^* values of 2.72 and 1.36 F/cmVs,³¹ respectively, demonstrating the potential of LPBT in organic electronic devices. However, the intrinsic charge transport properties of LPBT are yet to be investigated as are the possible effects of N-alkyl substitution to create derivatives of this π -conjugated ladder polymer backbone.

Here, we report the synthesis of a new ladder poly (6-methylpyrrolo[3,2-b:4,5-b']benzothiazine) (LPBT-Me) along with the parent LPBT (Chart 1). We also report detailed investigations of their molecular geometry, electronic structure, thin-film microstructure, and optical and field-effect charge transport properties. Our choice of the pyrrolobenzothiazine ladder structure as a model system to study the impacts of alkyl side chains on the chain conformation, electronic structure, and charge transport properties is based on the promise of the pyrrolobenzothiazine backbone³² and ladder polymer²⁹ as a class of p-type semiconducting materials. Furthermore, the N-H provides a molecular handle for ready attachment of diverse side chains, including solubilizing groups that may enable solution processing in organic solvents.³⁴ In the present study, a methyl group was chosen because it is the simplest example of an alkylated ladder polymer that still allows good solubility in protic acids. We probed the chain conformation and molecular geometry of LPBT and LPBT-Me in protic acid solutions by doing variable temperature optical absorption spectroscopy and via density functional theory (DFT) and time-dependent DFT calculations on ladder polymer chains of varying degrees of protonation. We show that the π -conjugated backbone of ladder poly(pyrrolobenzothiazine) has a donoracceptor motif that is very sensitive to protonation in acidic solvents but gives rise to a small bandgap (1.5 eV) that is unaffected by N-methylation. The thin-film microstructure of the LPBTs was characterized by grazing incidence wide-angle X-ray scattering (GIWAXS). We investigated the charge

transport properties of the LPBTs using the organic field-effect transistor (OFET) platform.

EXPERIMENTAL METHODS

Materials and Methods. 2,5-Diamino-1,4-benzenedithiol HCl monomer purchased from Ambeed with 97% purity was recrystallized in 20% HCl solution according to the published procedure before use. 33 2,3-Dibromo-N-methylmaleimide (99%) and 2,3-dibromomaleimide (99%) were purchased from Ambeed and used as received. Polyphosphoric acid (PPA, 84% P_2O_5), phenylphosphonic acid (PhPA), methanesulfonic acid (MSA) (>99%), formic acid, and triflic acid were purchased from Sigma-Aldrich and used as received. Methanol was purchased from Fisher Scientific and used as received. All reactions were performed under inert atmosphere.

The intrinsic viscosities $[\eta]$ of the polymers in MSA solutions were measured by an Ubbelohde viscometer, which was held at 30 °C using a water bath. The concentrations of the polymer solutions were chosen such that the elution time of the polymer solution was 1.1-1.8 times that of the pure solvent.

The 1H NMR spectrum was recorded on a Bruker AV500 instrument (at 500 MHz) using deuterated nitromethane/GaCl₃ as the solvent. Thermogravimetric analysis (TGA) was conducted on a TA Instruments model Q50 TGA. A heating rate of 10 °C/min under a flow of $\rm N_2$ was used with runs conducted from room temperature to 880 °C. Differential scanning calorimetry (DSC) analysis was performed on a TA Discovery DSC 500 under $\rm N_2$ by scanning from -10 to 350 °C at a heating and cooling rate of 10 °C/min. Optical absorption spectra were measured on a PerkinElmer model Lambda 900 UV—vis/near-IR spectrophotometer. Solution absorption spectra were obtained from dilute (10^{-5} – 10^{-6} M) solutions in methanesulfonic acid, formic acid, and triflic acid.

Cyclic voltammetry (CV) experiments were performed using an EG&G Princeton Applied Research potentiostat/galvanostat (model 273A). A three-electrode cell was used, using a platinum wire as the counter electrodes and the polymers coated onto platinum wires from MSA solution as the working electrodes. The reference electrode was Ag/AgNO₃ in acetonitrile. The acidic solvents were removed by dipping the substrates in isopropanol (IPA) overnight and subsequently dried in a vacuum oven at 60 °C. The supporting electrolyte solution consisted of 0.1 M tetrabutylammonium hexafluorophosphate (Bu₄NPF₆) in anhydrous acetonitrile. The electrolyte was purged with nitrogen for 15 min prior to the scans to ensure inert and anhydrous conditions. The reduction and oxidation potentials were referenced to the Fc/Fc+ couple by using ferrocene as an internal standard. Lowest unoccupied molecular orbital (LUMO) energy levels were estimated using the ferrocene value of -4.8 eV with respect to vacuum level. 38,39 The LUMO and HOMO levels were determined using the equations E_{LUMO} = $-(eE_{\text{red}}^{\text{onset}} + 4.8)$ and $E_{\text{HOMO}} = -(eE_{\text{ox}}^{\text{onset}} + 4.8)$.

Fourier transform infrared (FTIR) spectroscopy experiments were performed on a PerkinElmer Frontier spectrometer using free-standing films. The resolution was set at 1 cm⁻¹ and a set of 16 scans was averaged. Raman spectroscopy of the free-standing films was carried out on a Thermo Scientific DXR2 Raman microscope. A 532 nm laser with a power of 5 mW was focused on a sample through a 50x objective lens.

Grazing incidence wide-angle X-ray scattering (GIWAXS) measurements were conducted at the Advanced Light Source (ALS) at Lawrence Berkley National Laboratory by using beamlines 7.3.3 and a Pilatus 2 M area detector. The images were taken with a beam energy of 10 keV and an incidence angle of 0.14 with 5 s exposure time. Data were processed using Nika and WAXStools⁴⁰ in Igor Pro. Peak positions were determined by Lorentzian peak fittings. The crystal coherence length (L_c) of samples was determined by using the Scherrer equation: $^{41}L_c=2\pi K/\Delta q$, where K is a shape factor (typically 0.9) and Δq is the full width at half-maximum (fwhm) of the diffraction peak. Here, the L_c (100) and L_c (010) were obtained, respectively, from the fwhm of the (100) diffraction peak in the in-

Scheme 1. Synthesis of LPBT and LPBT-Me (PPA = Polyphosphoric Acid, 84% free P₂O₅; PhPA = Phenylphosphonic Acid)

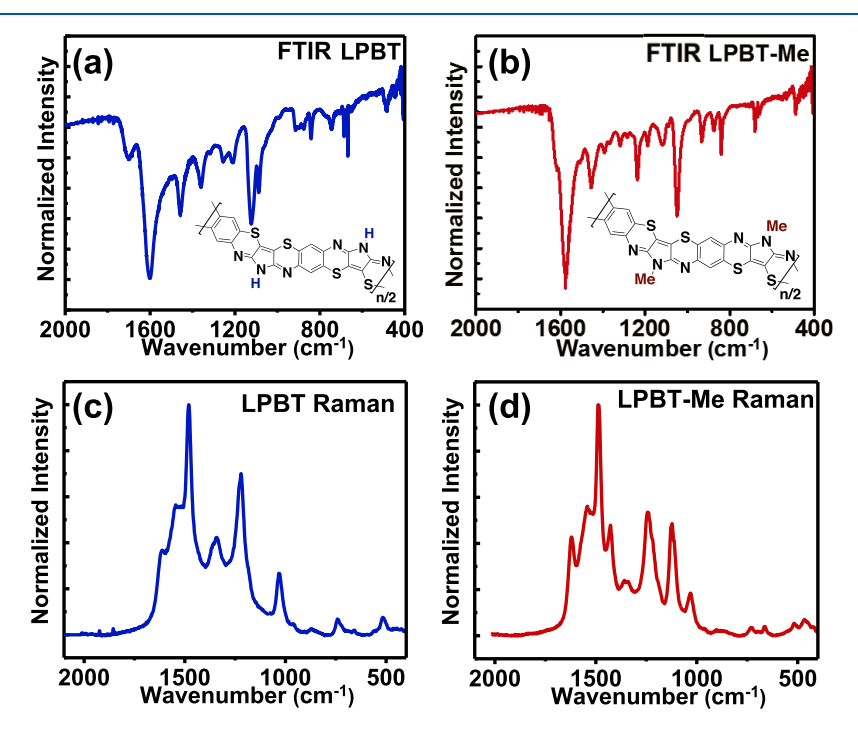


Figure 1. Normalized (a) FTIR and (c) Raman spectra for the free-standing films of LPBT, and normalized (b) FTIR and (d) Raman spectra for the free-standing films of LPBT-Me.

plane (q_{xy}) line-cut and the fwhm of the (010) diffraction peak in the out-of-plane (q_z) line-cut.

Gas-phase molecule density functional theory (DFT) and time-dependent density functional theory (TD-DFT) calculations were performed using the Gaussian 16 suit of programs 42 at the $\omega B97XD/631\text{-}G(d,p)$ level of theory on the representative oligomers comprising three repeat units. Vertical electronic transitions were calculated for 12 excited states.

Synthesis of LPBT-Me. PPA (42.90 g) was placed in a reaction vessel equipped with a mechanical stirrer, heated to 150 °C, and purged with nitrogen overnight. The PPA was cooled to 40 °C, and 2,5-diamino-1,4-benzenedithiol HCl (2.73 g, 11.2 mmol) was added. The temperature was increased to 70 °C and stirred for 24 h under nitrogen followed by 3 h under vacuum to complete the dehydrochlorination. The temperature was then reduced to 65 °C and 2,3-dibromo-*N*-methylmalemide (3.0 g, 11.2 mmol) was added and stirred overnight. The temperature was increased to 120 °C and stirred for 24 h. The temperature was then slowly increased to 180 °C and stirred for 72 h. The reaction mixture was cooled to room temperature, and methanol was added to quench the reaction. The polymer was filtered, washed with methanol, and dried. The crude

polymer was further purified by reprecipitation from MSA into methanol and thoroughly dried at 100 °C under a vacuum (2.12 g, 80%). Intrinsic viscosity: 1.7 dL/g (30.0 °C, MSA). Anal. Calcd for $C_{11}H_5N_3S_2$ (%): C, 54.30; H, 2.07; N, 17.27; S, 26.36; found (%): C, 50.71; H, 2.15; N, 15.49.

Synthesis of LPBT. The polymerization was carried out according to the same procedure as LPBT-Me, except a binary solvent mixture of PPA:PhPA was used in a 1:1 ratio (28.056/28.056 g). 2,5-Diamino-1,4-benzenedithiol HCl (2.50 g, 10.20 mmol), 2,3-dibromo-1H-maleimide (2.60 g, 10.20 mmol); (yield, 1.38 g, 60%). Intrinsic viscosity: 2.4 dL/g (30.0 °C, MSA). Anal. Calcd for $C_{10}H_3N_3S_2$ (%): C, 52.38; H, 1.32; N, 18.33; S, 27.97; found (%): C, 50.24; H, 1.82; N, 15.69.

RESULTS AND DISCUSSION

Synthesis and Characterization. The synthetic routes to both LPBT and LPBT-Me are shown in Scheme 1, and the detailed polymerization procedures are described in the Experimental Methods. The parent polymer LPBT was synthesized in a binary acid mixture using polyphosphoric

acid (PPA, 84% P_2O_5) and phenylphosphonic acid (PhPA) in a 1:1 wt. ratio according to the published procedure.³⁰ The addition of PhPA as a co-solvent was to enhance the solubility of the 2,3-dibromo-1*H*-malemide monomer in the PPA reaction medium and thus to prevent sublimation of the monomer at temperatures >80 °C.³⁰ Nevertheless, we still observed sublimation of the 2,3-dibromo-1*H*-malemimide monomer at high temperatures >80 °C, which means that the stoichiometry of the condensation polymerization is suboptimal. The sublimation of the monomer limited the intrinsic viscosity ([η]) of the LPBT sample to 2.4 dL/g in methanesulfonic acid (MSA) at 30 °C, which is similar to the previously reported polymer ([η] value of 3.7 dL/g in MSA at 25 °C).³⁰

The alkylated polymer LPBT-Me was synthesized in pure PPA since the co-solvent PhPA did not seem to improve the solubility of the maleimide monomer in the LPBT synthesis. When the temperature of the polymerization mixture was increased beyond 150 °C, the evaporation of 2,3-dibromo-N-methylmaleimide ($T_{\rm m}=120$ °C) was observed. This indicates that the solubility of the methylated monomer in PPA is still too low to afford high-molecular-weight polymers. Thus, the resulting LPBT-Me sample had a modest intrinsic viscosity [η] value of 1.7 dL/g in MSA at 30 °C. The moderate intrinsic viscosity values of both LPBT and LPBT-Me clearly highlight the limitations of the reaction scheme whereby the poor solubility of 2,3-dibromomaleimide monomers in acid media limits the molecular weight of achieved ladder polymers.

Both polymers were isolated as brown solids and are soluble in strong acids, such as MSA and triflic acid. The polymers form good quality thin films when spin-coated from MSA solutions, giving blue-green thin films with shiny lusters. LPBT and LPBT-Me can also be made into high-quality free-standing films, which were used to confirm the molecular structures of the polymers using Fourier transform infrared (FTIR) and Raman spectroscopy. The detailed procedure for forming the free-standing films is presented in the Supporting Information. The free-standing films were then used to characterize the molecular structures and thin-film microstructures. The FTIR and Raman spectra (Figure 1a-d) were analyzed alongside density functional theory (DFT) simulated FTIR and Raman spectra calculated at the ω B97XD/6-31G(d,p) level of theory on oligomers comprising three repeat units each (Figure S1ad). The peak positions and assigned vibrational modes are summarized in Tables S1 and S2 for LPBT and LPBT-Me, respectively.

The FTIR spectrum of the parent polymer LPBT (Figure 1a) has prominent aromatic $\nu(C=C)$ stretches at 1698 cm⁻¹ and high-intensity imine carbon–nitrogen stretches, $\nu(C=N)$ and $\nu(C-N)$, at 1600 and 1225 cm⁻¹, respectively. At lower wavenumbers, mixed pyrrole stretches can be seen at 1459, 1360, and 1124 cm⁻¹. Furthermore, the medium intensity carbon–sulfur $\nu(C-S)$ stretch is found at 1085 cm⁻¹.⁴³ Raman absorption bands for LPBT (Figure 1c) show sharp aromatic ν (C=C) stretches at 1611 and 1482 cm⁻¹, and high-intensity imine $\nu(C=N)$ stretches at 1545 cm⁻¹. Mixed pyrrole stretches are seen as a high-intensity band at 1349 cm⁻¹. The peak at 1235 cm⁻¹ can be assigned to mixed skeletal vibrations, and carbon-sulfur $\nu(C-S)$ stretches are found at lower wavenumbers at 1032 and 743 cm⁻¹.⁴³ We note that the FTIR stretches seen for LPBT are in good agreement with the previously reported infrared spectrum.³⁰

LPBT-Me shows similar FTIR stretches compared with the parent polymer (Figure 1b). The bands representing the aromatic $\nu(C=C)$ stretches are shown at 1613 cm⁻¹. The sharp band at 1577 cm⁻¹ originates from imine carbonnitrogen $\nu(C=N)$ stretches and the medium intensity peak at 1239 cm⁻¹ is from mixed pyrrole and $\nu(C-N)$ vibrations. The ν (C-S) stretching frequency is found at 1046 cm⁻¹.⁴³ Raman absorption bands for LPBT-Me (Figure 1d) show highintensity $\nu(C=C)$ stretches at 1619 and 1488 cm⁻¹ and a sharp imine stretching $\nu(C=N)$ band at 1542 cm⁻¹. Mixed pyrrole and aromatic vibrations are assigned to the peaks at 1428, 1362, and 1253 cm $^{-1}$. Finally, the $\nu(C-S)$ stretches are seen at 1026 and 737 cm $^{-1}$. The observed FTIR and Raman spectra of both LPBT and LPBT-Me are in good agreement with the DFT-calculated spectra (Figure S1a,d) and provide strong evidence for the molecular structures of both ladder polymers.

We note that the DFT-calculated Raman spectra show higher intensity stretches for LPBT-Me relative to LPBT (Figure S1c,d); this indicates greater polarizability (α) of the methylated polymer (α = 1946.4 au) compared to the parent polymer (α = 1799.6 a.u). The DFT-calculated dipole moment values were found to be 5.64 and 4.84 D for LPBT-Me and LPBT, respectively. In donor—acceptor π -conjugated systems, the intramolecular charge transfer (ICT) character is partially determined by a combination of polarizability and dipole moment, where larger dipole moments and polarizability typically indicate stronger ICT interactions. Therefore, the increased polarizability and dipole moment values for LPBT-Me suggest that methylation enhances the ICT character in pyrrolobenzothiazine ladder polymers.

To further characterize the molecular structures of the polymers, we have collected ¹H NMR spectra for both LPBT-GaCl₃ and LPBT-Me-GaCl₃ complexes in deuterated nitromethane⁴⁷ and the spectra are shown in Figure S2. Solutions of both polymers were prepared in deuterated nitromethane containing GaCl₃ according to the known procedures. 46 However, we point out the use of the Lewis-acid solutions as NMR solvents is known to produce impurities in the NMR spectra; 25,47 these impurities appear at \sim 5.9 ppm, and \sim 6.3– 6.5 ppm for both polymers (Figure S2). The NMR spectra show two main peaks from the benzene protons at 7.2 and 8.1 ppm for LPBT, and a cluster of peaks ~7.7-8.6 ppm for LPBT-Me. The cluster of peaks for LPBT-Me could be due to the planar/nonplanar conformational variations of the LPBT-Me backbone. The methyl peak is seen at 4.1 ppm, which overlaps with the deuterated nitromethane solvent peak at 4.5

The thermal stabilities of LPBT and LPBT-Me were probed using thermal gravimetric analysis (TGA) and differential scanning calorimetry (DSC) and the thermograms are shown in Figure S3a,b in the Supporting Information. Both polymers show excellent thermal stability measured by TGA (Figure S3a) with high thermal decomposition temperatures >450 °C and retain >65% of their mass at 800 °C. DSC scans revealed no phase transitions in the range of 25–350 °C (Figure S3b), which is typical for ladder polymers to have very high glass transition temperatures over 350 °C. 47

Electronic Structure of Ladder Poly-(pyrrolobenzothiazine)s. We investigated the electronic structures of LPBT and LPBT-Me by density functional theory (DFT) calculations, time-dependent DFT (TD-DFT) calculations, and cyclic voltammetry. The results of the DFT and

TD-DFT calculations performed at the ω B97XD/6-31G(d,p) level of theory and are aimed at gaining insight into the backbone geometries and frontier molecular orbital distributions and are shown in Figure 2a,b. The excited state geometry

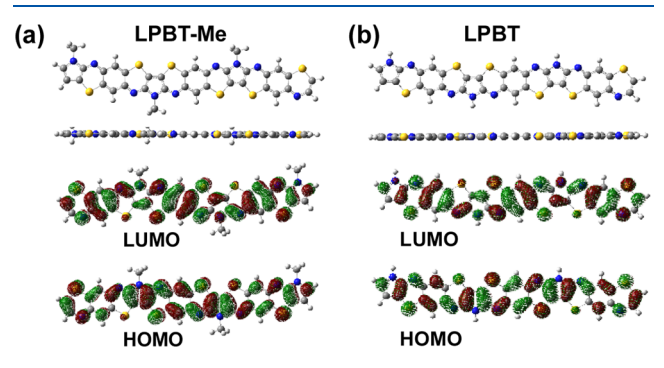


Figure 2. DFT calculations using the ω B97XD/6-31G(d,p) level of theory for the optimized ground state geometry and molecular orbital distributions for single oligomers comprising 3 repeat units each for (a) LPBT-Me and (b) LPBT. The molecular geometry top and side views are of the same single oligomer.

and vertical electronic excitations for 12 excited states are shown in Figure S4. The optimized ground state geometries of LPBT-Me (Figure 2a) and LPBT (Figure 2b) in the gas phase are completely coplanar with both HOMO and LUMO molecular orbitals delocalized across three repeat units. In the excited state, both LPBT and LPBT-Me show planar backbones with electronic transitions between 380 and 1330 nm. The optical bandgaps obtained from the DFT results show $E_{\rm g}^{\rm opt} \sim 1.0$ eV for LPBT and 0.9 eV for LPBT-Me. In the visible range, the oscillator strengths for the electronic transitions are more than twice as large for LPBT compared to LPBT-Me (Figure S4). Oscillator strengths often rise with increasing molecular planarity and rigidity in π -conjugated molecular systems; this suggests that LPBT maintains a rigid backbone upon photoexcitation, which is likely due to intramolecular hydrogen bonding.⁵⁰ The distance between the pyrrole proton and the imine nitrogen in LPBT was calculated to be 2.70 Å in the ground state and 2.67 Å in the exited state, which are less than the sum of their van der Waals radii (N, 1.55 Å; H, 1.20 Å). In fact, the shorter hydrogen-bonding distance in the excited state implies stronger hydrogen bonds relative to those in the ground state. Effects of intramolecular hydrogen bonding are also seen in the reorganization energy (λ) calculated for each oligomer upon hole injection. The reorganizational energy is the energy associated with geometry changes when going from a neutral to a charged-state geometry. 52,53 The λ values of 0.77 and 1.30 eV calculated for LPBT and LPBT-Me, respectively, show a 2-fold decrease for LPBT. This means that intramolecular hydrogen bonding may be crucial in maintaining rigidity upon charge injection for the ladder poly(pyrrolobenzothiazine)s.⁴⁸

We used cyclic voltammetry (CV) to measure the oxidation and reduction potentials of the polymers from which we derived the HOMO and LUMO energies, and the results are summarized in Table 1. The oxidation and reduction waves of LPBT and LPBT-Me thin films coated on platinum wires were measured in 0.1 M tetrabutylammonium hexafluorophosphate (Bu_4NPF_6) in degassed acetonitrile with $Ag/AgNO_3$ as the reference electrode and are shown in Figure 3, and additional

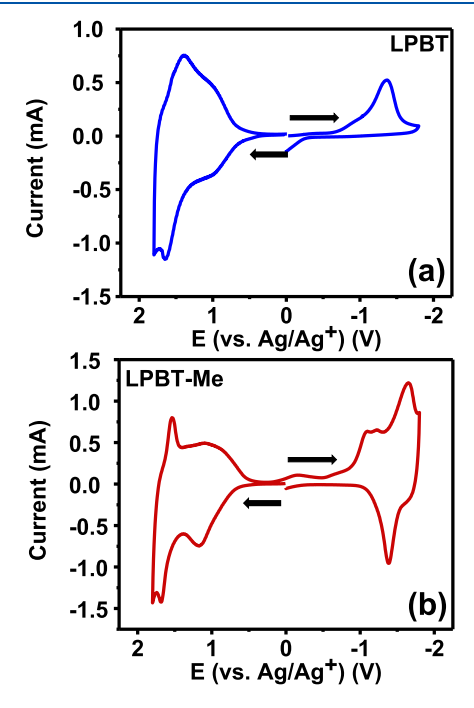


Figure 3. Cyclic voltammograms for the oxidation and reduction processes of (a) LPBT and (b) LPBT-Me thin films measured in a 0.1 M $\mathrm{Bu_4NPF_6}$ electrolyte solution using $\mathrm{Ag/AgNO_3}$ as the reference electrode. The scan rate was $100~\mathrm{mV/s}$. The arrows indicate the direction of charging.

scans are shown in Figure S5. LPBT shows two quasi-reversible oxidation waves at 0.97 and 1.40 V, and one nonreversible reduction wave centered at -1.36 V (Figure 3a). The onset oxidation potential of 0.66 V and onset reduction potential of -0.99 V were used to estimate the HOMO and LUMO energy levels of -4.96 and -3.27 eV, respectively, for LPBT. The electrochemical bandgap ($E_{\rm g}^{\rm elec.}$) of LPBT is thus 1.69 eV. The onset oxidation potential of 0.66 V is comparable to the previously reported value of 0.67 V. 30

The methylated polymer, LPBT-Me, also shows two quasi-reversible oxidation waves at 1.06 and 1.53 V (Figure 3b); however, unlike the parent polymer that showed a non-reversible reduction scan, LPBT-Me has a quasi-reversible reduction wave at -1.38 V. The quasi-reversibility of the LPBT-Me reduction wave suggests that the electron transfer process (n-doping) and the resulting radical anion are stabilized due to the methylation of the pyrrole nitrogen. The HOMO and LUMO levels were calculated from the onset oxidation potential and onset reduction potential at 0.59 and

Table 1. Electronic Structure Parameters and Optical Properties of LPBT and LPBT-Me

polymer	HOMO (eV)	LUMO (eV)	$E_{\rm g}^{\rm elec.} ({\rm eV})$	λ_{\max}^{a} (nm)	λ_{\max}^{b} (nm)	λ_{\max}^{c} (nm)	$\alpha_{\rm max}^{c} ({\rm cm}^{-1})$	$E_{ m g}^{\;{ m opt.}c}\;({ m eV})$
LPBT	-4.96	-3.27	1.69	933	960	676	2.89×10^{5}	1.49
LPBT-Me	-5.05	-3.46	1.56	936	993	663	2.25×10^{5}	1.51

^aSolution in MSA. ^bSolution in triflic acid. ^cSpin-coated thin films from MSA solution.

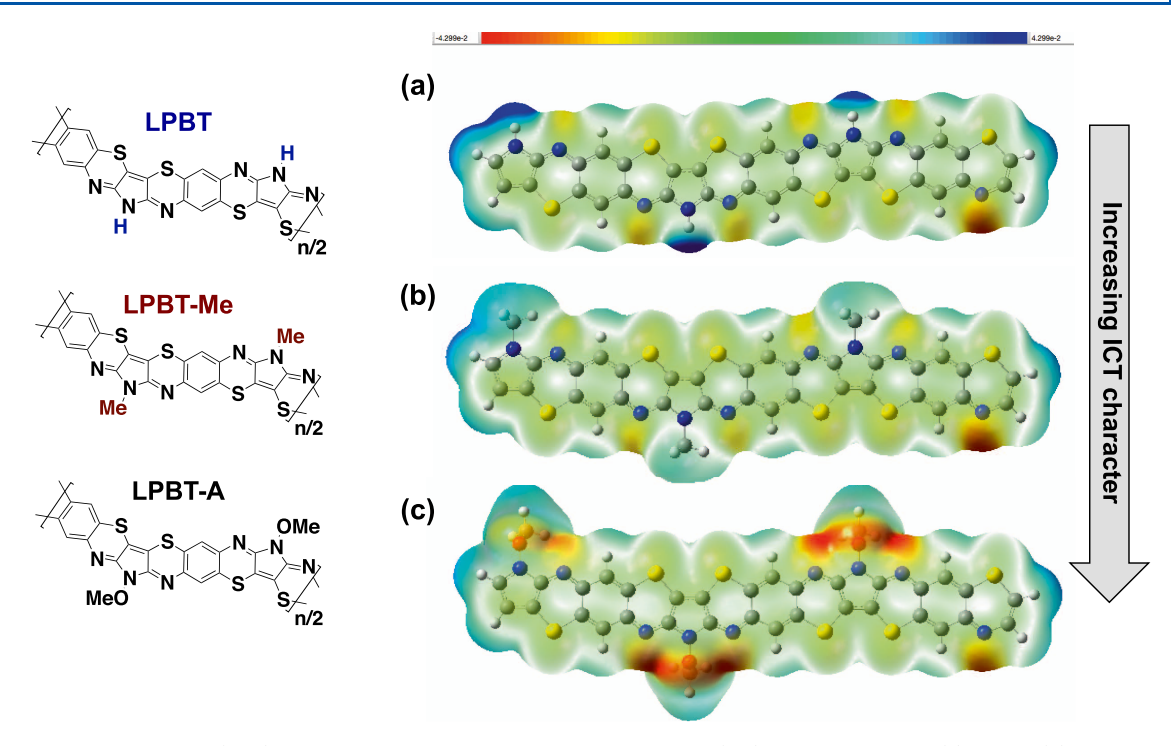


Figure 4. Electrostatic potential (ESP) map calculated using the DFT ω B97XD/6-31G(d,p) level of theory for (a) LPBT, (b) LPBT-Me, and (c) a theoretical oligomer with a methoxy group, LPBT-A.

-1.09 V, respectively, and are found to be -5.05 eV for the HOMO and -3.46 eV for the LUMO. Hence, the $E_{\rm g}^{\rm elec.}$ for LPBT-Me is 1.56 eV; this is 0.13 eV smaller than for LPBT. Additionally, alkylation decreases the HOMO energy level by 0.09 eV, and the LUMO level by 0.19 eV. This reduction in the LUMO level and stabilization of the electron injection and transfer process is explained by changes in electron density in the pyrrolobenzothiazine backbone, which is discussed below.

Electrostatic potential (ESP) maps for each oligomer were calculated using DFT at the ω B97XD/6-31G(d,p) level to visualize the charge distribution with respect to the difference between positive and negative charges on the oligomer backbones (Figure 4). 54-56 A theoretical oligomer bearing a strong electron-donating methoxy group (LPBT-A) was included in the calculation. Increasing the electron-donating ability of the substituent (hydrogen < methyl < methoxy) revealed a trend of increasing electron localization and intramolecular charge transfer (ICT) character in the polymer backbone. In LPBT, slight regions of negative charge (redorange) are centered on the imine nitrogens and sulfurs of the thiazine moieties, and more positively charged (blue) and neutral (green) regions are found on the pyrrole and benzene moieties (Figure 4a). This spatial localization of the electron density on thiazine implies intramolecular charge transfer (ICT) interactions 55,56 between the electronically coupled thiazine and pyrrole/benzene moieties whereby positive charges (holes) are transferred from the benzene and pyrrole moieties to the thiazine moieties. The effect is enhanced in LPBT-Me; methylation of the pyrrole nitrogen increases the electron density around thiazine, which explains the lower LUMO energy level and stabilization of the electron injection and transfer process.⁵⁷ The more negative ESP value of the imine nitrogen indicates its increased basicity (Figure 4b). The effect is more pronounced in the theoretical oligomer LPBT-A, which has the largest electron cloud on the thiazine nitrogens and has the most ICT character of the series (Figure 4c). The

alkylation-induced enhancement in the electron density of the imine nitrogens also means that LPBT-Me has improved solubility in protic acids, which is consistent with our experimental observations that LPBT-Me has improved solubility in acids.

Optical Absorption Spectra and Molecular Geometry in Protic Acid Solutions. The optical absorption spectra of the ladder polymers in MSA solutions are shown in Figure 5, and the lowest-energy peak positions are summarized in Table 1. To corroborate our spectroscopic results and gain a deeper understanding of the optical features seen in both polymers, DFT calculations were run at the ω B97XD/6-31G(d,p) level of theory on oligomers bearing +1, + 2, and +6 protonation states with the corresponding positive charge on the imine nitrogens (Figures 6 and S6). We note that it is more energetically favorable to protonate the imine nitrogens compared to the sulfur sites, ⁵⁸ and thus imine protonation was chosen for the calculations.

In MSA solution (Figure 5a), LPBT has two well-resolved high-energy bands at 354 nm ($\varepsilon_{\rm max}=1.05\times10^4~{\rm M}^{-1}~{\rm cm}^{-1}$) and 502 nm ($\varepsilon_{\rm max}=1.06\times10^4~{\rm M}^{-1}~{\rm cm}^{-1}$), of which the latter can be assigned to the $\pi-\pi^*$ transition. The intense lowest-energy absorption band centered at 933 nm originates from protonation-enhanced intramolecular charge transfer. This phenomenon is seen in many imine nitrogen-containing π -conjugated polymers in protic acid solutions where the ICT band is significantly red-shifted relative to the $\pi-\pi^*$ band. The effects of protonation on the ICT band are corroborated with DFT calculations shown in Figure S6a, which show protonation (+1 and +6 protonation states) induces spatial localization of the HOMO and LUMO molecular orbitals that correspond to the ICT character seen in the optical absorption spectra. 57,62,63

The optical absorption spectrum of LPBT-Me in MSA solution in Figure 5a shows features similar to those of the parent LPBT. The spectrum shows two high-energy peaks at

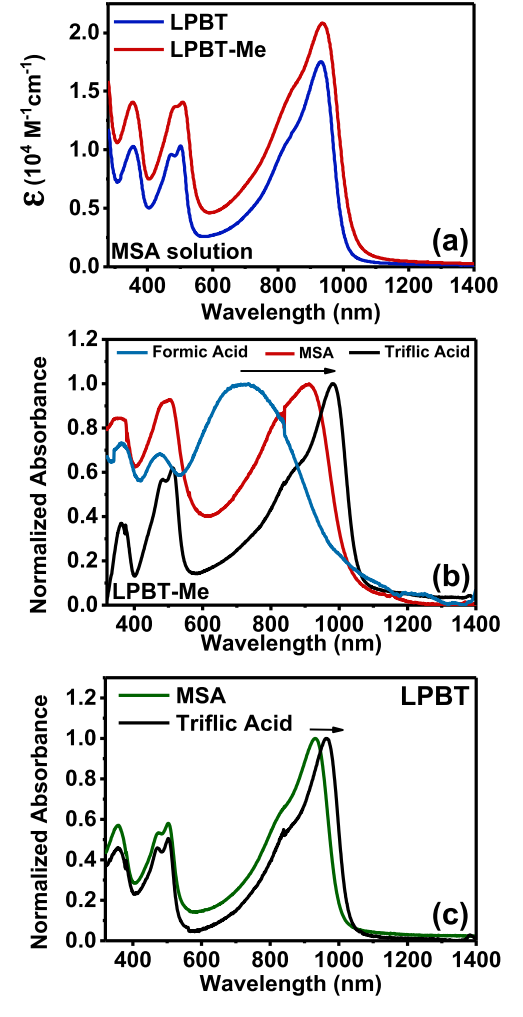


Figure 5. Optical absorption spectra of the ladder polymers (a) in the MSA solution. Normalized absorption spectra in dilute (10^{-6} M) protic acid solutions of varying p $K_{\rm a}$ values: (b) LPBT-Me and (c) LPBT.

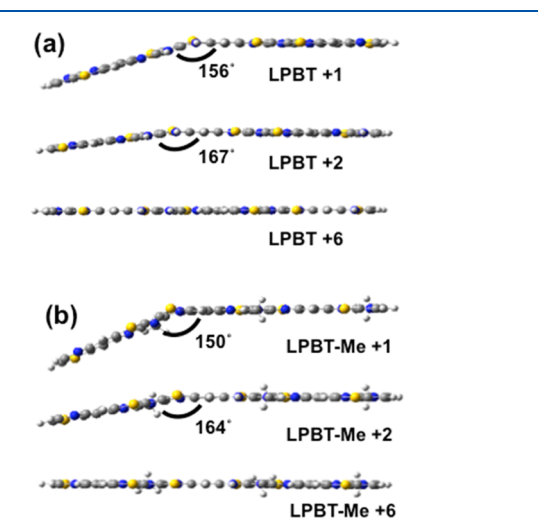


Figure 6. DFT-calculated optimized geometries of oligomers bearing +1, +2, and +6 protonation states for (a) LPBT and (b) LPBT-Me, where both oligomers were protonated on the imine nitrogens. Calculations were performed at the ω B97XD/6-31G(d,p) level of theory.

352 nm ($\varepsilon_{\rm max} = 1.51 \times 10^4~{\rm M}^{-1}~{\rm cm}^{-1}$) and 508 nm ($\varepsilon_{\rm max} = 1.38 \times 10^4~{\rm M}^{-1}~{\rm cm}^{-1}$), and a lowest-energy peak at 936 nm. Similar to LPBT, the peaks at 508 and 936 nm represent the $\pi - \pi^*$ transition and ICT band, respectively. The ICT band has the same origins as the parent LPBT, which was seen in the DFT calculations of the protonated oligomers (Figure S6b).

To understand the effects of the protonation on the ICT bands, optical absorption spectra were collected in dilute protic acid solutions of varying pKa values shown in Figure 5b,c. 47,58,64 The optical absorption spectra of LPBT-Me show that as the pK_a of the acid solvent decreases (formic acid, 3.75 > MSA, -1.9 > triflic acid, <math>-14.7), the ICT band (Figure 5b) red-shifts from formic acid ($\lambda_{\text{formic acid}} = 721 \text{ nm}$) to triflic acid ($\lambda_{\text{triflic acid}} = 993 \text{ nm}$), with increasing vibronic features and spectral narrowing. LPBT has a trend similar to that from MSA ($\lambda_{MSA} = 933 \text{ nm}$) to triflic acid ($\lambda_{triflic acid} = 960$ nm) (Figure 5c), except that LPBT is insoluble in formic acid. This means that the imine nitrogens are apparently not basic enough to abstract hydrogen from formic acid, which is in agreement with the DFT calculations (see the ESP map, Figure 4) that showed decreased electron density around the imine nitrogens. We propose that these trends are caused by (1) protonation-enhanced differences in electron density distributions on the π -conjugated backbones, resulting in variable stiffness of the polymer chain, and (2) intra- and intermolecular hydrogen-bonding interactions (or lack thereof in the case of LPBT-Me). When partially protonated in formic acid (p $K_a = 3.75$) or MSA (p $K_a = -1.9$), the polymer chains preferentially adopt nonplanar backbone conformations. This was observed in DFT calculations on optimized oligomers protonated at the imine nitrogens bearing +1, + 2, or +6 charges that resulted in out-of-plane bending deformations between the thiazine and pyrrole moieties that decreased as the protonation state increased (Figure 6a,b). Similar phenomena have been seen for other protonated rigid-chain polymers such as poly(p-phenylenebenzobis(oxazole)) (PBO) and poly(p-phenylenebenzobis(oxazole))phenylenebenzobis(thiazole)) (PBTZ) in ab initio calculations⁵⁸ and molecular dynamics studies.⁶⁵ However, LPBT shows a smaller degree of bending deformations (+1 protonation state, 156) relative to LPBT-Me (+1 pronation state, 150), which implies that LPBT is more rigid than LPBT-Me. Both intra- and intermolecular H-bonding interactions likely contribute to the improved rigidity of LPBT. In triflic acid (p $K_a = -14.7$), both polymers are almost fully protonated and preferentially adopt more planar backbone conformations, although they still retain strong ICT interactions (Figure S6). The optical absorption spectra of LPBT-Me compared to those of LPBT exhibit a 3 and 20 nm red shift in MSA and triflic acid, respectively (Figure 5b,c), which corroborates the enhanced protonation-enhanced ICT character observed in the DFT calculations (Figure S6). The results are also in agreement with the CV measurements, which showed that LPBT-Me has a lower LUMO energy level.

Variable temperature absorption spectra in dilute (10⁻⁵ M) triflic acid and MSA solutions (Figure 7a–e) were collected for temperatures between 20 and 100 °C to gauge the rigidity of the protonated ladder polymer backbones. As the temperature increases, the ICT band of the LPBT absorption spectrum in MSA solutions blue-shifts from 933 to 920 nm with accompanying spectral broadening and decreased absorbance (Figure 7a,f). In triflic acid, a blue shift is not observed; however, the absorption band weakens with increasing temperature (Figure 7b,f). The absorption spectrum of MSA

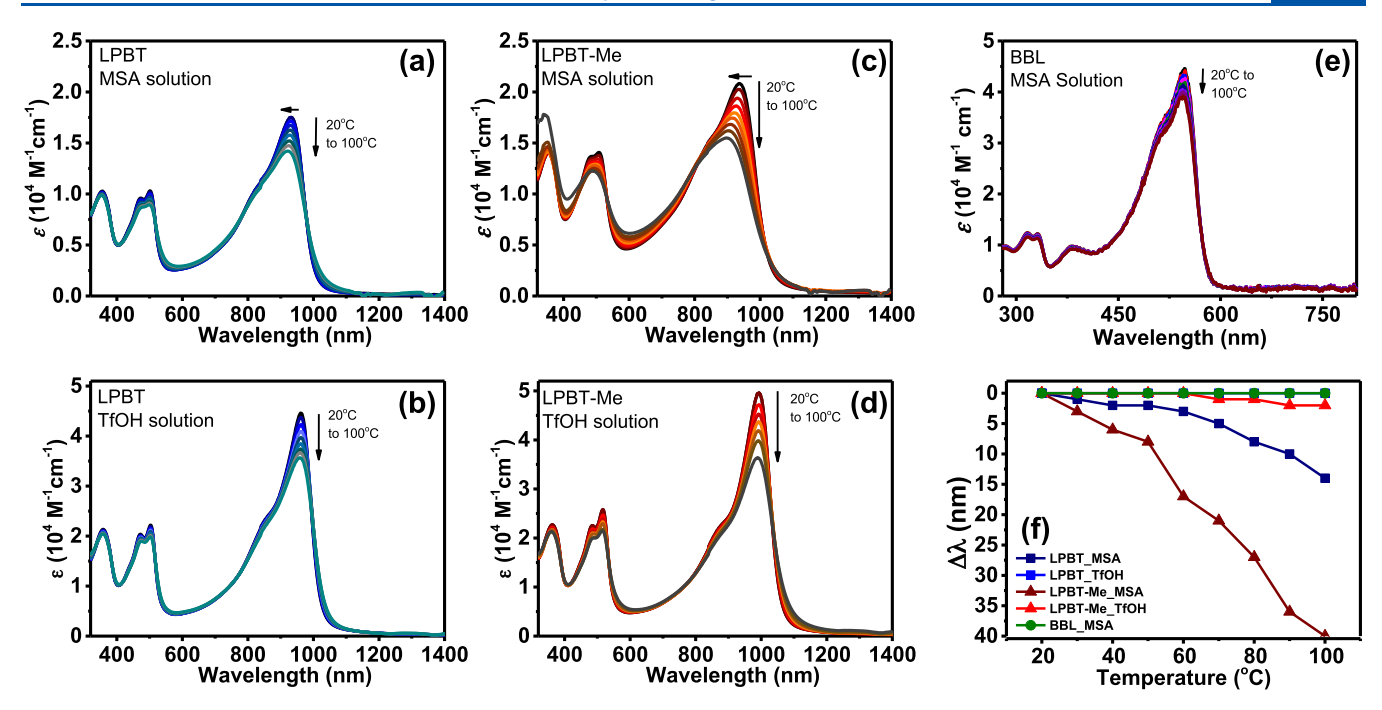


Figure 7. Variable temperature optical absorption spectra of LPBT in (a) MSA and (b) triflic acid solutions (10^{-5} M), LPBT-Me in (c) MSA and (d) triflic acid solutions (10^{-5} M), (e) BBL in MSA solution (10^{-5} M), and (f) the blue shifts of the maximum wavelengths with increasing temperature for LPBT, LPBT-Me, and BBL in MSA solutions and LPBT and LPBT-Me in triflic acid solutions.

solutions of LPBT-Me shows that the ICT band undergoes a large decrease in absorbance with spectral broadening accompanied by a sizable blue shift from 936 to 898 nm upon heating (Figure 7c,f). In contrast, triflic acid solutions of LPBT-Me undergo a small blue shift from 993 to 991 nm and a small decrease in molar absorptivity (Figure 7d,f). The observed changes in position, intensity, and structure of the ICT bands of both polymers can be understood to arise from thermally accessible conformation distributions. These changes are particularly evident in the MSA solutions; at higher temperatures, the ensembles of the polymer chains on average will be more distorted and nonplanar. The nonplanar chain geometries will decrease the average degree of conjugation as reflected in the blue-shifted, spectrally broadened, and weakened ICT bands.

BBL shows no thermochromism or conformational disorder (Figure 7e,f) due to the rigidity of the protonated ladder poly(benzimidazobenzophenanthroline) backbone, 13 which is in contrast to the ladder polymers studied here that both show thermochromic responses (Figure 7). The effects of protonation state on the polymers' molecular geometry are apparent in optical absorption spectra in triflic acid (Figure 7b,d,f) that show the geometry of the near fully protonated polymers are not sensitive to temperature changes such that there are no accompanying blue shifts for LPBT, and minimal blue shifts for LPBT-Me (2 nm), which is what is observed in the BBL spectrum in MSA solution (Figure 7e,f). Also, it is evident that alkylation causes increased conformational disorder (Figure 7a,c). The differences in conformational disorder can be explained in terms of π -electron delocalization and hydrogenbonding interactions. The protonation-enhanced spatial separation of the HOMO and LUMO molecular orbitals (i.e., the ICT interactions) (Figure S6) helps explain the conformational disorder in the polymers^{62,66,67} owing to the well-known fact that charge delocalization increases π -bond character across the polymer backbone and strengthens the

bonds within π -systems.⁶⁸ In triflic acid, in which the polymer chains are more fully protonated, the electron density is more delocalized thereby increasing the rigidity of the π -conjugated backbone. Therefore, increased electron delocalization in LPBT (Figure 4) in combination with the hydrogen bonding interactions increases the stiffness of the polymer backbone.

Although both LPBT and LPBT-Me exhibit thermochromism in solutions, whereas BBL does not, they are to a much lesser degree than many other semiflexible polymers including alkylated polythiophenes, ^{68,69} polyphenylene derivatives, ⁶⁹ poly(phenylenevinylene), ⁷⁰ and others. ¹ Thus, we can conclude that while the double-stranded ladder architecture explored here has not eliminated structural fluctuations, it has suppressed them compared to the single-stranded polymer architecture. It is likely that the complete electron delocalization and lack of ICT character in BBL previously shown by DFT calculations ²⁵ enhances its rigidity in protic acids. Indeed, the protonation-enhanced flexibility of the ladder backbone does impact the solid-state morphology and charge transport properties, which are discussed below.

Solid-State Optical Properties. The thin-film absorption spectra of LPBT and LPBT-Me were collected from thin films spin-coated onto glass substrates from MSA solutions. The detailed procedure is described in the Supporting Information. The thin-film absorption spectra are shown in Figure 8, and the optical parameters (absorption coefficient (α) , absorption maximum (λ_{\max}) , and optical bandgaps $(E_{\rm g}^{\rm opt.})$) are summarized in Table 1.

The thin-film absorption spectrum of LPBT (Figure 8) has bands in the 300–850 nm range with an absorption coefficient (α) of 2.78 × 10⁵ cm⁻¹ at the lowest-energy absorption band maximum ($\lambda_{\rm max}$) of 749 nm. At the $\lambda_{\rm max}$ value of 676 nm, the $\alpha_{\rm max}$ value is 2.89 × 10⁵ cm⁻¹. The intense absorption band has vibronic peaks at 676 and 749 nm. The optical bandgap ($E_{\rm g}^{\rm opt.}$) of LPBT measured from the onset of thin-film absorption is 1.49 eV, which is identical to the previously reported bandgap

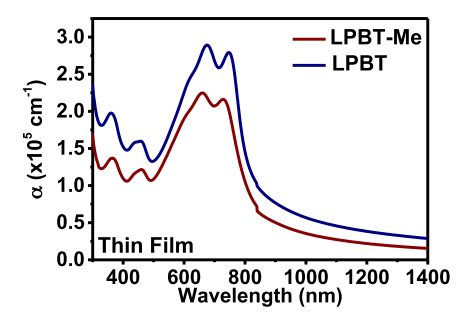


Figure 8. Optical absorption spectrum of the ladder polymers spin-coated from MSA solutions onto glass substrates.

of 1.51 eV for LPBT.³⁰ Compared to the absorption spectrum of LPBT in the MSA solution (Figure 5a), the solid-state absorption spectrum is distinctly different. First, the MSA solution spectrum with the lowest-energy peak at 933 nm is substantially red-shifted from the thin-film absorption spectrum (with the lowest-energy peak at 749 nm). This 174 nm red shift of the absorption spectrum due to protonation confirms the enhancement of the ICT character of the LPBT backbone in MSA solution. Second, the vibronic structure of the main absorption band in the solid state is significantly enhanced compared to what is observed in the MSA solution absorption; this difference can be understood by the much more rigid chains in the solid state.

The thin-film absorption spectrum of LPBT-Me (Figure 8) is very similar to that of the parent LPBT; it spans the 300–840 nm region with the main absorption band centered at 731 nm ($\alpha = 2.16 \times 10^5 \text{ cm}^{-1}$) (Table 1); the lowest-energy absorption λ_{max} at 663 nm has an α_{max} value of 2.25 × 10⁵ cm⁻¹. The absorption edge optical bandgap of LPBT-Me is 1.51 eV, which is similar to that of the parent LPBT. The DFT-calculated optical bandgaps of LPBT and LPBT-Me ($E_g^{\text{opt.}} \sim 0.9-1.0 \text{ eV}$) are significantly smaller compared to those obtained experimentally, which is a commonly seen phenomenon in the bandgaps calculated for extended π -systems and

are typically attributed to deficiencies of many density functional methods. $^{70-72}$ We note that while the electrochemical bandgap ($E_{\rm g}^{\rm elec.}=1.56~{\rm eV}$) of LPBT-Me derived from cyclic voltammetry measurements discussed above is 0.13 eV smaller than that of LPBT ($E_g^{\text{elec.}} = 1.69 \text{ eV}$), the optical bandgaps of LPBT and LPBT-Me are nearly identical. The larger difference between the electrochemical bandgap and optical bandgap in LPBT (0.2 eV) compared to LPBT-Me (0.06 eV) indicates that LPBT has a greater effective exciton binding energy (E_b) . A decreased E_b value in the methylated polymer likely arises in part from the previously discussed stronger ICT effect and a larger calculated dipole moment in LPBT-Me (μ = 5.64 D) compared with LPBT (μ = 4.84 D). 73-75 However, the main difference in the thin-film absorption spectrum of the N-methyl polymer, LPBT-Me, compared to that of LPBT is that the lowest-energy absorption band is broadened [full width at half-maximum (fwhm) = 297 nm] compared to the fwhm = 289 nm in LPBT. This is an indication of increased disorder in the LPBT-Me thin film relative to that of LPBT. These results corroborate the previously discussed DFT calculations that show that the parent polymer has larger oscillator strengths in the simulated absorption spectra (Figure S4) and a nearly 2-fold decrease in the reorganizational energies ($\lambda_{LPBT} = 0.77$ eV and $\lambda_{LPBT-Me} =$ 1.3 eV).

Thin-Film Microstructures of LPBT and LPBT-Me. Two-dimensional grazing incidence wide-angle X-ray scattering (2D-GIWAXS) was employed to examine the thin-film microstructures of LPBT and LPBT-Me ladder polymers. The 2D-GIWAXS diffraction patterns along with the corresponding one-dimensional (1D) linecuts in both the out-of-plane (OOP) and in-plane (IP) directions are shown in Figure 9. The diffraction peak position (q), interplanar spacings (d), crystalline coherence length (L_c) , and paracrystallinity disorder (g) are summarized in Table 2.

LPBT thin films exhibited a pronounced (010) diffraction peak centered at $q_z = 1.86 \text{ Å}^{-1}$ in the out-of-plane (OOP)

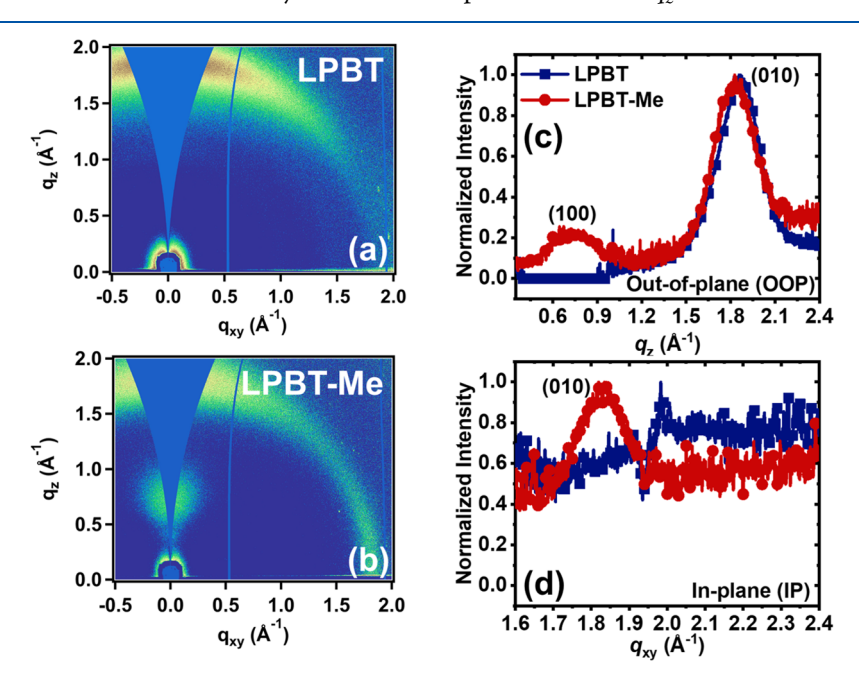


Figure 9. 2D-GIWAXS diffraction patterns of LPBT (a) and LPBT-Me (b) thin films; 1D linecuts of GIWAXS patterns in the out-of-plane (OOP) direction (c) and the in-plane (IP) direction (d).

Table 2. Summary of Diffraction Peak Position (q), Interplanar Spacing (d), Crystalline Coherence Length (L_c) , Number of Stacked Layers within a Crystallite (N), and Paracrystallinity Disorder (g) of LPBT and LPBT-Me Thin Films

polymer	$q_{z,(010) \text{ OOP}} (\text{Å}^{-1})$	$d_{\pi-\pi}$ (Å)	$L_{\rm c,(010)~OOP}~({ m nm})$	number of layers $(N_{\pi-\pi})$	<i>g</i> _π (%)	$q_{z,(100) \text{ OOP}} (Å^{-1})$	d_{lam} (Å)
LPBT	1.860	3.38	1.39	5.1	18.6		
LPBT-Me	1.834	3.43	1.20	4.5	20.2	0.742	8.46

direction, corresponding to a π - π packing distance of 3.38 Å (Table 2), which is identical to the previously reported $\pi - \pi$ packing distance of ~ 3.4 Å.³⁰ The L_c values and the gparameter of LPBT in the π -stacking direction were found to be 1.39 nm and 18.6%, respectively (Table 2). In the case of LPBT-Me, a distinct (010) diffraction peak at $q_z = 1.83 \text{ Å}^{-1}$ was accompanied by a (100) diffraction peak at $q_z = 0.74 \text{ Å}^{-1}$ in the OOP direction. As a result, the $\pi-\pi$ packing distance and the lamellar distance of LPBT-Me chains were calculated to be 3.43 and 8.46 Å, respectively (Table 2). The slightly large $d_{\pi-\pi}$ of LPBT-Me relative to that of LPBT can be attributed to the more disordered LPBT-Me backbone, which would prevent the polymer chains from approaching each other and stacking tightly. The $L_{c,(010)}$ value of LPBT-Me was 1.20 nm, which corresponds to about 4 layers of chains stacked along the π -direction within one crystallite, which is slightly smaller than that of LPBT, which features up to 5 consecutive layers of chains per crystallite (Table 2). Furthermore, LPBT-Me was found to exhibit a slightly higher degree of lattice disorder, g_{π} = 20.2%, relative to the parent LPBT. These subtle differences in the microstructures of LPBT and LPBT-Me suggest a more disordered nature in the methylated polymer, which collectively has implications for charge transport properties, as discussed below.

Field-Effect Charge Transport Properties of LPBT and LPBT-Me. We investigated the charge transport properties of LPBT and LPBT-Me by using bottom-gate/top-contact organic field-effect transistor (OFETs) devices, and the output and transfer curves are shown in Figure 10, whereas the numerical hole transport properties are summarized in Table 3.

The average saturation region hole mobility (μ_h) of LPBT was found to be $(3.10 \pm 0.39) \times 10^{-3}$ cm²/(V s), and the average threshold voltage (V_T) was calculated to be $-44.6 \pm$ 3.1 V (Table 3). The maximum μ_h of LPBT was 3.74×10^{-3} $cm^2/(V s)$, which is about an order of magnitude lower than that extracted from previously reported OECT measurements.³¹ The hole mobility of the methylated counterpart, LPBT-Me, was decreased by over 2-fold to an average value of $(1.30 \pm 0.21) \times 10^{-3} \ \text{cm}^2/(\text{V s})$ and a maximum value of 1.64 \times 10⁻³ cm²/(V s) (Table 3). The average $V_{\rm T}$ value of LPBT-Me was -42.9 ± 3.4 V and comparable to that of LPBT. Moreover, the on/off current ratio ($I_{\rm on}/I_{\rm off}$) of LPBT ($I_{\rm on}/I_{\rm off}$ $\sim 10^3$) was about an order of magnitude higher than that of LPBT-Me $(I_{on}/I_{off} \sim 10^2)$. These results indicate that methylation has negative effects on the macroscopic charge transport properties of the class of conjugated ladder poly(pyrrolobenzothiazine)s.

Given the similar polymer molecular weights, comparable HOMO energy levels, and semiconductor bandgaps of LPBT and LPBT-Me, the 2-fold mobility gap could be attributed to the more disordered nature of LPBT-Me. We propose that the increased conformational disorder in LPBT-Me compared to LPBT might not only disrupt intrachain hole delocalization, as evidenced by the more localized HOMO orbital distributions seen in LPBT-Me (Figure S6) but also interfere with tight interchain packing, as discussed earlier, both of which resulted

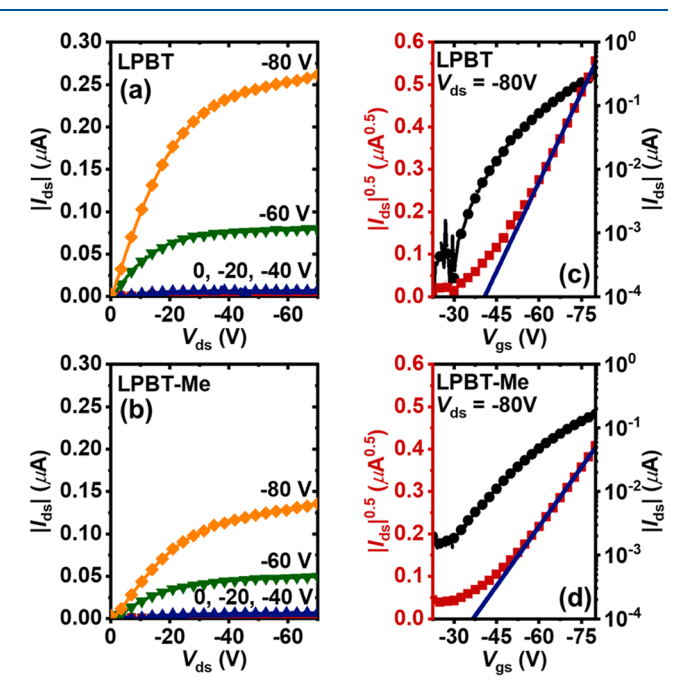


Figure 10. (a, b) Output curves of p-channel organic field-effect transistor (OFET) devices of LPBT (a) and LPBT-Me (b) ladder polymers. (c, d) Transfer curves of p-channel OFET devices of LPBT (c) and LPBT-Me (d) ladder polymers measured in saturated regimes $(V_{\rm ds} = -80~{\rm V})$.

in the observed poor hole mobility of LPBT-Me. We note that the hole mobility of both LPBT and LPBT-Me remains relatively modest compared to several state-of-the-art p-type semiconducting polymers. The inferior hole transport properties can be rationalized by the low polymer molecular weight and the flexible polymer backbone. Nevertheless, the LPBT and LPBT-Me backbone holds tremendous potential to become the prototypical p-type semiconducting ladder polymer if the polymer synthesis protocol could be improved to suppress monomer sublimation by solvent engineering such that higher polymer molecular weights can be obtained. Incorporating much longer side chains to potentially induce liquid crystalline ordering of the poly(pyrrolobenzothiazine) backbone is another approach that could improve the charge transport properties of this class of ladder polymers. 80

CONCLUSIONS

We have synthesized the new p-type semiconducting LPBT-Me and the known LPBT and used them to investigate the effects of N-alkyl substitution on the chain conformation, electronic structure, and charge transport properties of ladder poly(pyrrolobenzothiazine)s. The LPBTs were found to be a class of small-bandgap polymer semiconductors, whose optical bandgap of 1.5 eV is unchanged by N-alkyl side chain substitution. The π -conjugated backbone of the ladder LPBTs was found to exhibit a donor—acceptor architecture that facilitates enhanced intramolecular charge transfer (ICT) upon

Table 3. Hole Transport Properties of LPBT and LPBT-Me Conjugated p-Type Ladder Polymers Measured by Organic Field-Effect Transistors

polymer	$\mu_{\text{ave}}^{a} (10^{-3} \text{ cm}^{2}/(\text{V s}))$	$\mu_{\rm max} \; (10^{-3} \; {\rm cm^2/(V \; s)})$	$V_{\mathrm{T}}^{}}\left(\mathrm{V}\right)$	$I_{ m on}/I_{ m off}^{c}$
LPBT	3.10 ± 0.39	3.74	-44.6 ± 3.1	$(1.4 \pm 0.9) \times 10^3$
LPBT-Me	1.30 ± 0.21	1.64	-42.9 ± 3.4	$(6.1 \pm 2.7) \times 10^2$

 $[^]a\mu_{\rm ave}$, average field-effect hole mobility (\pm one standard deviation). bV_v , average threshold voltage (\pm one standard deviation). $^cI_{\rm on}/I_{\rm off}$ on/off current ratio. Average values and standard deviations were calculated from at least 15 different devices.

protonation in acid solutions. Partial protonation of either LPBT or LPBT-Me gives rise to a more flexible backbone evidenced by thermochromism and confirmed by planar/nonplanar chain conformation variation with degree of protonation seen in DFT calculations.

Our GIWAXS characterization of the thin-film microstructures of LPBT and LPBT-Me shows that *N*-methyl substitution results in an increased $\pi-\pi$ stacking distance, reduced crystallinity, and increased lattice disorder. The average field-effect hole mobility decreased from 3.1×10^{-3} cm²/(V s) in LPBT to 1.3×10^{-3} cm²/(V s) in LPBT-Me, which is likely limited by the relatively low molecular weights of these ladder polymers. The observed factor of 2.4 difference in carrier mobility between LPBT and LPBT-Me could be explained by the differences in their thin-film microstructures and DFT-predicted reorganization energies.

ASSOCIATED CONTENT

Supporting Information

The Supporting Information is available free of charge at https://pubs.acs.org/doi/10.1021/acs.macromol.3c01561.

Preparation of thin films on glass and free-standing films, fabrication and characterization of OFET devices, DFT-calculated FTIR and Raman spectra and their peak assignments, proton NMR spectra, TGA and DSC scans, TD-DFT-calculated vertical electronic transitions and optimized geometries, additional CV scans, and HOMO and LUMO molecular orbitals for protonated oligomers (PDF)

AUTHOR INFORMATION

Corresponding Author

Samson A. Jenekhe — Department of Chemistry, University of Washington, Seattle, Washington 98195-1750, United States; Department of Chemical Engineering, University of Washington, Seattle, Washington 98195-1750, United States; Orcid.org/0000-0002-0898-9541; Email: jenekhe@uw.edu

Author

Sarah M. West – Department of Chemistry, University of Washington, Seattle, Washington 98195-1750, United States

Duyen K. Tran – Department of Chemical Engineering, University of Washington, Seattle, Washington 98195-1750, United States; orcid.org/0000-0002-3065-6153

Jiajie Guo — Molecular Engineering and Sciences Institute, University of Washington, Seattle, Washington 98195, United States; orcid.org/0000-0001-9131-4352

Shinya E. Chen — Molecular Engineering and Sciences Institute, University of Washington, Seattle, Washington 98195, United States; Oorcid.org/0000-0001-8995-7500

David S. Ginger — Department of Chemistry, University of Washington, Seattle, Washington 98195-1750, United States; Occid.org/0000-0002-9759-5447

Complete contact information is available at: https://pubs.acs.org/10.1021/acs.macromol.3c01561

Notes

The authors declare no competing financial interest.

ACKNOWLEDGMENTS

This work was supported by the National Science Foundation (DMR-2003518). Part of this work was conducted at the Molecular Analysis Facility, a National Nanotechnology Coordinated Infrastructure (NNCI) site at the University of Washington with partial support from the National Science Foundation via awards NNCI-2025489 and NNCI-1542101. Part of this work was conducted using equipment in the Biomedical Diagnostic Foundry for Translational Research sponsored by the M.J. Murdock Charitable Trust. The DFT calculations were done through the use of advanced computational, storage, and networking infrastructure provided by the Hyak supercomputer system at the University of Washington. D.S.G., J.G., and S.E.C. acknowledge initial support from NSF DMR-2003456 and later support from NSF DMR-2309577. This research used beamline 7.3.3⁴¹ of the Advanced Light Source (ALS), which is a DOE Office of Science User Facility under contract no. DEAC02-05CH11231. The authors thank C. Zhu and E. Schaible at the ALS for assistance with GIWAXS data acquisition and analysis.

REFERENCES

- (1) Cao, Z.; Leng, M.; Cao, Y.; Gu, X.; Fang, L. How Rigid Are Conjugated Non-Ladder and Ladder Polymers? *J. Polym. Sci.* **2022**, *60* (3), 298–310.
- (2) Griggs, S.; Marks, A.; Bristow, H.; McCulloch, I. N-Type Organic Semiconducting Polymers: Stability Limitations, Design Considerations and Applications. *J. Mater. Chem. C* **2021**, 9 (26), 8099–8128.
- (3) Kim, F. S.; Park, C. H.; Na, Y.; Jenekhe, S. A. Effects of Ladder Structure on the Electronic Properties and Field-Effect Transistor Performance of Poly(Benzobisimidazobenzophenanthroline). *Org. Electron.* **2019**, *69*, 301–307.
- (4) Lee, J.; Kalin, A. J.; Yuan, T.; Al-Hashimi, M.; Fang, L. Fully Conjugated Ladder Polymers. *Chem. Sci.* 2017, 8 (4), 2503–2521.
- (5) Teo, Y. C.; Lai, H. W. H.; Xia, Y. Synthesis of Ladder Polymers: Developments, Challenges, and Opportunities. *Chem. Eur. J.* **2017**, 23 (57), 14101–14112.
- (6) Van Deusen, R. L. Benzimidazo-Benzophenanthroline Polymers. J. Polym. Sci., Part B: Polym. Lett. 1966, 4 (3), 211–214.
- (7) Babel, A.; Jenekhe, S. A. Electron Transport in Thin-Film Transistors From an n-Type Conjugated Polymer. *Adv. Mater.* **2002**, *14* (5), 371–374.
- (8) Babel, A.; Jenekhe, S. A. n-Channel Field-Effect Transistors from Blends of Conjugated Polymers. J. Phys. Chem. B 2002, 106 (24), 6129-6132.
- (9) Alam, M. M.; Jenekhe, S. A. Efficient Solar Cells from Layered Nanostructures of Donor and Acceptor Conjugated Polymers. *Chem. Mater.* **2004**, *16* (23), 4647–4656.

- (10) Jenekhe, S. A.; Yi, S. Efficient Photovoltaic Cells from Semiconducting Polymer Heterojunctions. *Appl. Phys. Lett.* **2000**, 77 (17), 2635–2637.
- (11) Sun, H.; Vagin, M.; Wang, S.; Crispin, X.; Forchheimer, R.; Berggren, M.; Fabiano, S. Complementary Logic Circuits Based on High-Performance n-Type Organic Electrochemical Transistors. *Adv. Mater.* **2018**, *30* (9), No. 1704916.
- (12) Surgailis, J.; Savva, A.; Druet, V.; Paulsen, B.; Wu, R.; Hamidi-Sakr, A.; Ohayon, D.; Nikiforidis, G.; Chen, X.; McCulloch, I.; Rivnay, J.; Inal, S. Mixed Conduction in an N-Type Organic Semiconductor in the Absence of Hydrophilic Side-Chains. *Adv. Funct. Mater.* **2021**, *31* (21), No. 2010165.
- (13) Wu, H.-Y.; Yang, C.-Y.; Li, Q.; Kolhe, N. B.; Strakosas, X.; Stoeckel, M.-A.; Wu, Z.; Jin, W.; Savvakis, M.; Kroon, R.; Tu, D.; Woo, H. Y.; Berggren, M.; Jenekhe, S. A.; Fabiano, S. Influence of Molecular Weight on the Organic Electrochemical Transistor Performance of Ladder-Type Conjugated Polymers. *Adv. Mater.* 2022, 34 (4), No. 2106235.
- (14) Babel, A.; Wind, J. D.; Jenekhe, S. A. Ambipolar Charge Transport in Air-Stable Polymer Blend Thin-Film Transistors. *Adv. Funct. Mater.* **2004**, *14* (9), 891–898.
- (15) Kim, F. S.; Ahmed, E.; Subramaniyan, S.; Jenekhe, S. A. Air-Stable Ambipolar Field-Effect Transistors and Complementary Logic Circuits from Solution-Processed n/p Polymer Heterojunctions. ACS Appl. Mater. Interfaces 2010, 2 (11), 2974–2977.
- (16) Alam, M. M.; Jenekhe, S. A. Conducting Ladder Polymers: Insulator-to-Metal Transition and Evolution of Electronic Structure upon Protonation by Poly(Styrenesulfonic Acid). *J. Phys. Chem. B* **2002**, *106* (43), 11172–11177.
- (17) Tam, T. L. D.; Lin, M.; Handoko, A. D.; Xu, J. Thermoelectric Performances of N-Doped Ladder-Type Conjugated Polymers Using Various Viologen Radical Cations. *ACS Appl. Polym. Mater.* **2021**, 3 (11), 5596–5603.
- (18) Wang, S.; Sun, H.; Ail, U.; Vagin, M.; Persson, P. O. Å.; Andreasen, J. W.; Thiel, W.; Berggren, M.; Crispin, X.; Fazzi, D.; Fabiano, S. Thermoelectric Properties of Solution-Processed n-Doped Ladder-Type Conducting Polymers. *Adv. Mater.* **2016**, 28 (48), 10764–10771.
- (19) Yang, C.-Y.; Stoeckel, M.-A.; Ruoko, T.-P.; Wu, H.-Y.; Liu, X.; Kolhe, N. B.; Wu, Z.; Puttisong, Y.; Musumeci, C.; Massetti, M.; Sun, H.; Xu, K.; Tu, D.; Chen, W. M.; Woo, H. Y.; Fahlman, M.; Jenekhe, S. A.; Berggren, M.; Fabiano, S. A High-Conductivity n-Type Polymeric Ink for Printed Electronics. *Nat. Commun.* **2022**, *13* (1), No. 1792
- (20) Volkov, A. V.; Sun, H.; Kroon, R.; Ruoko, T.; Che, C.; Edberg, J.; Muller, C.; Fabiano, S.; Crispin, X. Asymmetric Aqueous Supercapacitor Based on P- and n-Type Conducting Polymers. *ACS Appl. Energy Mater.* **2019**, 2 (8), 5350–5355.
- (21) Guo, J.; Flagg, L. Q.; Tran, D. K.; Chen, S. E.; Li, R.; Kolhe, N. B.; Giridharagopal, R.; Jenekhe, S. A.; Richter, L. J.; Ginger, D. S. Hydration of a Side-Chain-Free n-Type Semiconducting Ladder Polymer Driven by Electrochemical Doping. *J. Am. Chem. Soc.* **2023**, 145 (3), 1866–1876.
- (22) Briseno, A. L.; Mannsfeld, S. C. B.; Shamberger, J. P.; Ohuchi, F. S.; Bao, Z.; Jenekhe, S. A.; Xia, Y. Self-Assembly, Molecular Packing, and Electron Transport in n-Type Polymer Semiconductor Nanobelts. *Chem. Mater.* **2008**, 20 (14), 4712–4719.
- (23) Nayak, K.; Mark, J. E. Chain Packing in Two Aromatic Heterocyclic Polymers, One of Which Has a Ladder Structure. *Makromol. Chem.* **1986**, *187* (6), *1547*–1550.
- (24) Song, H. H.; Fratini, A. V.; Chabinyc, M.; Price, G. E.; Agrawal, A. K.; Wand, C.-S.; Burkette, J.; Dudis, D. S.; Arnold, F. E. Crystal Structure and Thin Film Morphology of BBL Ladder Polymer. *Synth. Met.* **1995**, *69* (1–3), 533–535.
- (25) West, S. M.; Tran, D. K.; Guo, J.; Chen, S. E.; Ginger, D. S.; Jenekhe, S. A. Phenazine-Substituted Poly-(Benzimidazobenzophenanthrolinedione): Electronic Structure, Thin Film Morphology, Electron Transport, and Mechanical

- Properties of an n-Type Semiconducting Ladder Polymer. *Macromolecules* **2023**, *56* (5), 2081–2091.
- (26) Imai, K.; Kurihara, M.; Mathias, L.; Wittmann, J.; Alston, W. B.; Stille, J. K. Synthesis and Properties of Thermally Stable Ladder Polymers Containing the 1,4-Pyrazine Ring Obtained from Polyheterocyclizations of Tetramines and Tetraketones in Poly(Phosphoric Acid) and m-Cresol. *Macromolecules* 1973, 6 (2), 158–162.
- (27) Sicree, A. J.; Arnold, F. E.; Deusen, R. L. V. New Imidazoisoquinoline Ladder Polymers. J. Polym. Sci., Polym. Chem. Ed. 1974, 12 (2), 265–272.
- (28) Gerber, A. H. Thermally Stable Polymers Derived from 2,3,5,6-Tetraaminopyridine. *J. Polym. Sci., Polym. Chem. Ed.* **1973**, 11 (7), 1703–1719.
- (29) Arnold, F. E. Ladder Polymers from Tetraaminodiquinoxalpyrene. J. Polym. Sci., Part A-1: Polym. Chem. 1970, 8 (8), 2079–2089.
- (30) Tam, T. L. D.; Lin, M.; Chien, S. W.; Xu, J. Facile Synthesis of Solubilizing a Group-Free, Solution-Processable p-Type Ladder Conjugated Polymer and Its Thermoelectric Properties. *ACS Macro Lett.* **2022**, *11* (1), 110–115.
- (31) Wu, X.; Tam, T. L. D.; Chen, S.; Salim, T.; Zhao, X.; Zhou, Z.; Lin, M.; Xu, J.; Loo, Y.-L.; Leong, W. L. All-Polymer Bulk-Heterojunction Organic Electrochemical Transistors with Balanced Ionic and Electronic Transport. *Adv. Mater.* **2022**, 34 (42), No. 2206118.
- (32) Leng, M.; Koripally, N.; Huang, J.; Vriza, A.; Lee, K. Y.; Ji, X.; Li, C.; Hays, M.; Tu, Q.; Dunbar, K.; Xu, J.; Ng, T. N.; Fang, L. Synthesis and Exceptional Operational Durability of Polyaniline-Inspired Conductive Ladder Polymers. *Mater. Horiz.* **2023**, *10* (10), 4354–4364.
- (33) Wolfe, J. F.; Loo, B. H.; Arnold, F. E. Rigid-Rod Polymers. 2. Synthesis and Thermal Properties of Para-Aromatic Polymers with 2,6-Benzobisthiazole Units in the Main Chain. *Macromolecules* **1981**, 14 (4), 915–920.
- (34) Hickl, P.; Ballauff, M.; Scherf, U.; Müllen, K.; Lindner, P. Characterization of a Ladder Polymer by Small-Angle X-Ray and Neutron Scattering. *Macromolecules* **1997**, *30* (2), 273–279.
- (35) Hong, W.; Wei, Z.; Xi, H.; Xu, W.; Hu, W.; Wang, Q.; Zhu, D. 6H-Pyrrolo[3,2-b:4,5-B']Bis[1,4]Benzothiazines: Facilely Synthesized Semiconductors for Organic Field-Effect Transistors. *J. Mater. Chem.* **2008**, *18* (40), 4814–4820.
- (36) Wei, Z.; Hong, W.; Geng, H.; Wang, C.; Liu, Y.; Li, R.; Xu, W.; Shuai, Z.; Hu, W.; Wang, Q.; Zhu, D. Organic Single Crystal Field-Effect Transistors Based on 6H-Pyrrolo[3,2-b:4,5-B']Bis[1,4]-Benzothiazine and Its Derivatives. *Adv. Mater.* **2010**, 22 (22), 2458–2462.
- (37) Wang, S.; Hong, W.; Ren, S.; Li, J.; Wang, M.; Gao, X.; Li, H. New Ladder-Type Conjugated Polymer with Broad Absorption, High Thermal Durability, and Low Band Gap. *J. Polym. Sci., Part A: Polym. Chem.* **2012**, *50* (20), 4272–4276.
- (38) Trasatti, S. The Absolute Electrode Potential: An Explanatory Note (Recommendations 1986). *Pure Appl. Chem.* **1986**, *58* (7), 955–966.
- (39) Pommerehne, J.; Vestweber, H.; Guss, W.; Mahrt, R. F.; Bässler, H.; Porsch, M.; Daub, J. Efficient Two Layer Leds on a Polymer Blend Basis. *Adv. Mater.* **1995**, 7 (6), 551–554.
- (40) Oosterhout, S. D.; Savikhin, V.; Zhang, J.; Zhang, Y.; Burgers, M. A.; Marder, S. R.; Bazan, G. C.; Toney, M. F. Mixing Behavior in Small Molecule:Fullerene Organic Photovoltaics. *Chem. Mater.* **2017**, 29 (7), 3062–3069.
- (41) Hexemer, A.; Bras, W.; Glossinger, J.; Schaible, E.; Gann, E.; Kirian, R.; MacDowell, A.; Church, M.; Rude, B.; Padmore, H. A SAXS/WAXS/GISAXS Beamline with Multilayer Monochromator. *J. Phys.: Conf. Ser.* **2010**, *247*, No. 012007.
- (42) Frisch, M. J.; Frisch, M. J.; et al. *Gaussian 16*, revision C.01; Gaussian, Inc.: Wallingford, CT, 2016.
- (43) Liu, G.; Fang, Q.; Xu, W.; Chen, H.; Wang, C. Vibration Assignment of Carbon-Sulfur Bond in 2-Thione-1,3-Dithiole-4,5-

- Dithiolate Derivatives. Spectrochim. Acta, Part A 2004, 60 (3), 541-550.
- (44) Yang, H.; Fan, H.; Wang, Z.; Yan, H.; Dong, Y.; Cui, C.; Ade, H.; Li, Y. Impact of Isomer Design on Physicochemical Properties and Performance in High-Efficiency All-Polymer Solar Cells. *Macromolecules* **2020**, 53 (20), 9026–9033.
- (45) Cui, Y.; Yao, H.; Gao, B.; Qin, Y.; Zhang, S.; Yang, B.; He, C.; Xu, B.; Hou, J. Fine-Tuned Photoactive and Interconnection Layers for Achieving over 13% Efficiency in a Fullerene-Free Tandem Organic Solar Cell. *J. Am. Chem. Soc.* **2017**, *139* (21), 7302–7309.
- (46) Yong Lee, J.; Kim, K. S.; Jin Mhin, B. Intramolecular Charge Transfer of π -Conjugated Push–Pull Systems in Terms of Polarizability and Electronegativity. *J. Chem. Phys.* **2001**, *115* (20), 9484–9489.
- (47) Roberts, M. F.; Jenekhe, S. A. Lewis-Acid Coordination-Complexes of Polymers. 3. Poly(Benzimidazobenzophenanthroline) Ladder and Semiladder Polymers. *Polymer* **1994**, 35 (20), 4313–4325
- (48) Mahmood, A.; Tang, A.; Wang, X.; Zhou, E. First-Principles Theoretical Designing of Planar Non-Fullerene Small Molecular Acceptors for Organic Solar Cells: Manipulation of Noncovalent Interactions. *Phys. Chem. Chem. Phys.* **2019**, *21* (4), 2128–2139.
- (49) Duan, R.; Han, G.; Qu, L. B.; Yi, Y. Importance of Molecular Rigidity on Reducing the Energy Losses in Organic Solar Cells: Implication from Geometric Relaxations of A–D–A Electron Acceptors. *Mater. Chem. Front.* **2021**, *5* (10), 3903–3910.
- (50) Vezie, M. S.; Few, S.; Meager, I.; Pieridou, G.; Dörling, B.; Ashraf, R. S.; Goñi, A. R.; Bronstein, H.; McCulloch, I.; Hayes, S. C.; Campoy-Quiles, M.; Nelson, J. Exploring the Origin of High Optical Absorption in Conjugated Polymers. *Nat. Mater.* **2016**, *15* (7), 746–753.
- (51) Kurbanova, A. M. Van Der Waals Radii of Elements. *Inorg. Mater.* **2001**, *37* (9), 15.
- (52) Brédas, J.-L.; Beljonne, D.; Coropceanu, V.; Cornil, J. Charge-Transfer and Energy-Transfer Processes in π -Conjugated Oligomers and Polymers: A Molecular Picture. *Chem. Rev.* **2004**, *104* (11), 4971–5004.
- (53) Zade, S. S.; Zamoshchik, N.; Bendikov, M. From Short Conjugated Oligomers to Conjugated Polymers. Lessons from Studies on Long Conjugated Oligomers. *Acc. Chem. Res.* **2011**, 44 (1), 14–24. (54) Murray, J. S.; Politzer, P. The Electrostatic Potential: An Overview. *Wiley Interdiscip. Rev.: Comput. Mol. Sci.* **2011**, 1 (2), 153–
- (55) Yao, H.; Cui, Y.; Qian, D.; Ponseca, C. S.; Honarfar, A.; Xu, Y.; Xin, J.; Chen, Z.; Hong, L.; Gao, B.; Yu, R.; Zu, Y.; Ma, W.; Chabera, P.; Pullerits, T.; Yartsev, A.; Gao, F.; Hou, J. 14.7% Efficiency Organic Photovoltaic Cells Enabled by Active Materials with a Large Electrostatic Potential Difference. *J. Am. Chem. Soc.* **2019**, *141* (19), 7743–7750.
- (56) Xia, H.; Xu, X.; Qian, C.; Guo, J.; Zhao, J.; Zhang, K.; Tan, H.; Peng, Q.; Zhu, Q. A-D-A-D-A-Type Oligomer versus A-D-A-Type Small Molecule: Synthesis and Advanced Effect of the D-A Repeat Unit on Morphology and Photovoltaic Properties. *ACS Appl. Energy Mater.* **2022**, *5* (3), 3146–3155.
- (57) Kim, B.-G.; Ma, X.; Chen, C.; Ie, Y.; Coir, E. W.; Hashemi, H.; Aso, Y.; Green, P. F.; Kieffer, J.; Kim, J. Energy Level Modulation of HOMO, LUMO, and Band-Gap in Conjugated Polymers for Organic Photovoltaic Applications. *Adv. Funct. Mater.* 2013, 23 (4), 439–445.
- (58) Farmer, B. L.; Dudis, D. S.; Adams, W. W. Calculation of the Effects of Protonation on Rigid-Rod Polymers. *Polymer* **1994**, *35* (17), 3745–3751.
- (59) Jenekhe, S. A.; Lu, L.; Alam, M. M. New Conjugated Polymers with Donor–Acceptor Architectures: Synthesis and Photophysics of Carbazole–Quinoline and Phenothiazine–Quinoline Copolymers and Oligomers Exhibiting Large Intramolecular Charge Transfer. *Macromolecules* **2001**, 34 (21), 7315–7324.
- (60) Agrawal, A. K.; Jenekhe, S. A. Synthesis and Processing of Heterocyclic Polymers as Electronic, Optoelectronic, and Nonlinear

- Optical Materials. 2. New Series of Conjugated Rigid-Rod Polyquinolines and Polyanthrazolines. *Macromolecules* **1993**, *26* (5), 895–905.
- (61) Zhang, Q. T.; Tour, J. M. Imine-Bridged Planar Poly-(Phenylenethiophene)s and Polythiophenes. J. Am. Chem. Soc. 1997, 119 (41), 9624–9631.
- (62) Hedström, S.; Henriksson, P.; Wang, E.; Andersson, M. R.; Persson, P. Temperature-Dependent Optical Properties of Flexible Donor–Acceptor Polymers. *J. Phys. Chem. C* **2015**, *119* (12), 6453–6463.
- (63) Onwubiko, A.; Yue, W.; Jellett, C.; Xiao, M.; Chen, H.-Y.; Ravva, M. K.; Hanifi, D. A.; Knall, A.-C.; Purushothaman, B.; Nikolka, M.; Flores, J.-C.; Salleo, A.; Bredas, J.-L.; Sirringhaus, H.; Hayoz, P.; McCulloch, I. Fused Electron Deficient Semiconducting Polymers for Air Stable Electron Transport. *Nat. Commun.* **2018**, *9* (1), No. 416.
- (64) Yang, C. J.; Jenekhe, S. A. Conjugated Aromatic Polyimines. 2. Synthesis, Structure, and Properties of New Aromatic Polyazomethines. *Macromolecules* **1995**, 28 (4), 1180–1196.
- (65) Farmer, B. L.; Chapman, B. R.; Dudis, D. S.; Adams, W. W. Molecular Dynamics of Rigid Rod Polymers. *Polymer* **1993**, 34 (8), 1588–1601.
- (66) Salaneck, W. R.; Inganäs, O.; Thémans, B.; Nilsson, J. O.; Sjögren, B.; Österholm, J.-E.; Brédas, J. L.; Svensson, S. Thermochromism in Poly(3-hexylthiophene) in the Solid State: A Spectroscopic Study of Temperature-dependent Conformational Defects. J. Chem. Phys. 1988, 89 (8), 4613–4619.
- (67) Roux, C.; Leclerc, M. Thermochromic Properties of Polythiophene Derivatives: Formation of Localized and Delocalized Conformational Defects. *Chem. Mater.* **1994**, *6* (5), 620–624.
- (68) Danielsen, S. P. O.; Davidson, E. C.; Fredrickson, G. H.; Segalman, R. A. Absence of Electrostatic Rigidity in Conjugated Polyelectrolytes with Pendant Charges. *ACS Macro. Lett.* **2019**, 8 (9), 1147–1152.
- (69) Roux, C.; Bergeron, J.-Y.; Leclerc, M. Thermochromic Properties of Polythiophenes: Structural Aspects. *Makromol. Chem.* **1993**, *194* (3), 869–877.
- (70) Hutchison, G. R.; Zhao, Y.-J.; Delley, B.; Freeman, A. J.; Ratner, M. A.; Marks, T. J. Electronic Structure of Conducting Polymers: Limitations of Oligomer Extrapolation Approximations and Effects of Heteroatoms. *Phys. Rev. B* **2003**, *68* (3), No. 035204.
- (71) Sun, H.; Autschbach, J. Electronic Energy Gaps for π -Conjugated Oligomers and Polymers Calculated with Density Functional Theory. *J. Chem. Theory Comput.* **2014**, *10* (3), 1035–1047
- (72) Jain, M.; Chelikowsky, J. R.; Louie, S. G. Reliability of Hybrid Functionals in Predicting Band Gaps. *Phys. Rev. Lett.* **2011**, *107* (21), No. 216806.
- (73) Wu, P.-T.; Kim, F. S.; Champion, R. D.; Jenekhe, S. A. Conjugated Donor—Acceptor Copolymer Semiconductors. Synthesis, Optical Properties, Electrochemistry, and Field-Effect Carrier Mobility of Pyridopyrazine-Based Copolymers. *Macromolecules* **2008**, *41* (19), 7021–7028.
- (74) Leenaers, P. J.; Maufort, A. J. L. A.; Wienk, M. M.; Janssen, R. A. J. Impact of π -Conjugated Linkers on the Effective Exciton Binding Energy of Diketopyrrole-Dithienopyrrole Copolymers. *J. Phys. Chem. C* **2020**, *124* (50), 27403–27412.
- (75) Izquierdo, M. A.; Broer, R.; Havenith, R. W. A. Theoretical Study of the Charge Transfer Exciton Binding Energy in Semiconductor Materials for Polymer:Fullerene-Based Bulk Heterojunction Solar Cells. *J. Phys. Chem. A* **2019**, *123* (6), 1233–1242.
- (76) Chen, Z.; Cai, P.; Chen, J.; Liu, X.; Zhang, L.; Lan, L.; Peng, J.; Ma, Y.; Cao, Y. Low Band-Gap Conjugated Polymers with Strong Interchain Aggregation and Very High Hole Mobility Towards Highly Efficient Thick-Film Polymer Solar Cells. *Adv. Mater.* **2014**, *26* (16), 2586–2591.
- (77) Park, S.; Lim, B. T.; Kim, B.; Son, H. J.; Chung, D. S. High Mobility Polymer Based on a π -Extended Benzodithiophene and Its Application for Fast Switching Transistor and High Gain Photoconductor. *Sci. Rep.* **2014**, *4* (1), No. 5482.

- (78) Kang, I.; Yun, H.-J.; Chung, D. S.; Kwon, S.-K.; Kim, Y.-H. Record High Hole Mobility in Polymer Semiconductors via Side-Chain Engineering. J. Am. Chem. Soc. 2013, 135 (40), 14896–14899.
- (79) Luo, L.; Huang, W.; Yang, C.; Zhang, J.; Zhang, Q. Recent Advances on π -Conjugated Polymers as Active Elements in High Performance Organic Field-Effect Transistors. *Front. Phys.* **2021**, *16* (3), No. 33500.
- (80) McCulloch, I.; Heeney, M.; Bailey, C.; Genevicius, K.; MacDonald, I.; Shkunov, M.; Sparrowe, D.; Tierney, S.; Wagner, R.; Zhang, W.; Chabinyc, M. L.; Kline, R. J.; McGehee, M. D.; Toney, M. F. Liquid-Crystalline Semiconducting Polymers with High Charge-Carrier Mobility. *Nat. Mater.* **2006**, *5* (4), 328–333.